The Orbit of the High-Mass X-Ray Binary Pulsar 1E 1145.1−6141

Paul S. Ray

E. O. Hulburt Center for Space Research, Code 7655, Naval Research Laboratory, Washington, DC 20375; Paul.Ray@nrl.navy.mil

and

Deepto Chakrabarty[1]

Department of Physics and Center for Space Research, Massachusetts Institute of Technology, Cambridge, MA 02139; deepto@space.mit.edu

ABSTRACT

Observations of the 297 s X-ray pulsar 1E 1145.1−6141 with the *Rossi X-Ray Timing Explorer* have revealed its 14.4 d eccentric orbit around its B supergiant companion. The best-fit orbital elements are: $P_{\rm orb} = 14.365(2)$ d, $a_x \sin i = 99.4(18)$ light s, $e = 0.20(3)$. No eclipses are detected, indicating that the binary inclination is $\lesssim 55°$.

Subject headings: binaries: close — pulsars: individual (1E 1145.1−6141) — stars: neutron — X-rays: stars

1. Introduction

It is a remarkable coincidence that there are two unrelated X-ray pulsars in Centaurus with nearly identical spin periods separated by only 15′ on the sky (White et al. 1978; Lamb et al. 1980). One of the sources is the 292 s transient X-ray pulsar 2S 1145−619, which is associated with the main sequence Be V companion Hen 715 (HD 102567) (Dower et al. 1978) and is 1.5 kpc distant. The pulsar exhibits periodic outbursts at 186.5 d intervals, which are believed to occur during periastron passage in the neutron star's eccentric orbit. The X-ray flux in quiescence is typically $\lesssim 3$ mcrab but the periastron flares reach a flux of several hundred mcrab.

[1]Alfred P. Sloan Research Fellow

The second source is the 297 s X-ray pulsar 1E 1145.1−6141, which is associated with the B2 Iae supergiant companion V830 Cen (Hutchings et al. 1981; Densham & Charles 1982) and is 8.5 ± 1.5 kpc distant. The pulsar appears to be persistent and steady, with a typical X-ray flux of a few mcrab, corresponding to a luminosity of order 10^{36} erg s^{-1}. Such a low luminosity is inconsistent with Roche-lobe overflow and indicates that the pulsar is almost certainly accreting from the wind of V830 Cen. A binary period of $\gtrsim 6$ d is required for the B supergiant to fit within the pulsar's orbit (Densham & Charles 1982), and previous authors have proposed periods ranging from 5.6 d to 12.1 d based on optical photometric and spectroscopic studies (Ilovaisky et al. 1982; Hutchings et al. 1987).

For supergiant X-ray binaries with orbital period $P_{\rm orb} \lesssim 20$ d, there is a significant *a priori* probability of an X-ray eclipse (corresponding to a critical binary inclination) given approximately by

$$\Pr \simeq 0.38 \left(\frac{P_{\rm orb}}{15\ {\rm d}}\right)^{-2/3} \left(\frac{M_c}{15 M_\odot}\right)^{-1/3} \left(\frac{R_c}{24 R_\odot}\right), \qquad (1)$$

where M_c and R_c are the companion's mass and radius, and we have assumed a circular orbit. Eclipsing X-ray pulsars provide important constraints on the neutron star mass range (van Kerkwijk et al. 1995). Since only 8 such systems are known (Chakrabarty et al. 2002; Corbet & Mukai 2002), it is of significant interest to increase the sample. Thus motivated, we observed 1E 1145.1−6141 with the *Rossi X-Ray Timing Explorer (RXTE)* in an effort to determine the pulsar's orbital period and search for X-ray eclipses. In this paper, we report our discovery of the 14.4 d orbit of 1E 1145.1−6141. We found no evidence for an X-ray eclipse.

2. Observations

Our observations were made using the Proportional Counter Array (PCA) on *RXTE* (Jahoda et al. 1996). This detector consists of five identical proportional counter units (PCUs), each containing a propane anticoincidence layer followed by several xenon/methane layers. It operates in the 2–60 keV range and has an effective area of ∼6500 cm^2 and a 1° field of view. In addition to the standard data modes, data were also collected in GoodXenon mode, which records the arrival time (1 μs resolution) and energy (256-channel resolution) of every non-vetoed event. To maximize the signal-to-noise ratio, we confined our analysis to events in the top xenon layer of each PCU and restricted the energy range to 2.5–10 keV.

We observed 1E 1145.1−6141 on multiple occasions between 1997 June and 2000 February. Our 1997 observations were each 20 ks long, while the 1998–2000 observations were short 3 ks observations at roughly daily intervals. A summary of these observations is given

in Table 1. In all cases, the observation epochs were selected to avoid periastron passages of 2S 1145−619 in order to prevent contamination by bright outbursts of this source. It is important to note that non-imaging timing observations can only resolve the coherent pulsations of 1E 1145.1−6141 and 2S 1145−619 into separate Fourier bins for observations lengths $\gtrsim$ 20 ks. Based on our long observations where the two nearby periodicities can be distinguished, in quiescence (i.e., away from its periastron), 2S 1145−619 does not interfere significantly with observations of 1E 1145.1−6141. The PCA energy spectrum for 1E 1145.1−6141 during the various observations was well fitted by an absorbed, cutoff power law spectral model. Using our 1997 June 30 observation (14.6 ks) as a typical example, the best-fit spectral parameters were: photon index $\Gamma = 1.24$, cutoff energy $E_c = 6.4$ keV, e-folding energy $E_f = 18$ keV, and equivalent hydrogen column density $N_{\rm H} = 3.3 \times 10^{22}$ cm^{-2}. These values are typical of the rest of our observations, but the source flux was variable by a factor of $\sim$2.

3. Timing Analysis

We binned the 2–10 keV events from each observation into a time series at 1 s resolution and converted to barycentric dynamical time (TDB) at the solar system barycenter. We folded the time series from each observation at a nominal pulse period of 296.5 s to form a 64-bin pulse profile and then cross-correlated each pulse profile with a high signal-to-noise template (see Figure 1) in order to derive a pulse arrival time for each observation. These arrival times can be compared to the time predicted by a constant-period model, using the best-fit pulse period determined for each of the four observation epochs. The resulting arrival time residuals are shown in Figure 2. There is clearly a roughly sinusoidal variation in the residuals with a period of about 14 days in the residuals, which we presume is due to orbital motion. We determined an initial orbital period using the measured minima in the arrival time residuals in Figure 2. Assuming a constant orbital period $P_{\rm orb}$, these five minima must be separated by integer multiples of $P_{\rm orb}$. The best-fit orbital period is thus $P_{\rm orb} = 14.37 \pm 0.02$ d.

In order to derive the remaining binary parameters and refine the orbital period determination, the effects of the binary motion must be decoupled from intrinsic changes in the pulsar's spin period due to accretion torques. We perfomed a combined fit of all of the arrival time measurements shown in Figure 2. Because of the effect of accretion torque during the time between observations we could not produce a fully phase-connected orbital fit. Instead, we used a model where the frequency and phase of the pulsar were allowed to jump discontinuously between each epoch of observation, while the orbital param-

eters applied globally. We performed this fit using the TEMPO pulsar timing package (see http://pulsar.princeton.edu/tempo). No frequency derivatives within each observation epoch were included in the model since local accretion torques seem to dominate on a timescale of days.

Our best-fit binary parameters are given in Table 2. This fit is shown in Figure 3. The errors quoted in Table 2 are statistical errors only; any biases introduced from the accretion torque are not included. However, these systematic errors should be reasonably small since the data cover more than six cycles of the binary orbit and such effects can be expected to average out.

With the orbit determined, we can determine the best fit pulsar spin frequency at each epoch with the orbital effects removed. These determinations are shown in Table 3, and Figure 4. In each case, we have fit a constant frequency model to determine the best average frequency for the epoch. In all cases there are significant deviations from this model. The errors shown are the single parameter standard deviations not including coupling to the other parameters which were held constant. For completeness, the historical measurements of the pulsar period are also included in the table. However, it should be noted that they are not corrected for the Doppler effect of the pulsar orbit and may be inconsistently corrected to the solar system barycenter. The pulsar projected orbital velocity is 150 km/s so the reported periods could differ from the intrinsic spin period by as much as 0.002 mHz.

The pulsar has shown significant spin up since its discovery in 1978. Fitting the frequencies to a straight line yields an average frequency derivative of 1.2×10^{-14} Hz/s. This implies a spin up timescale of 9×10^3 y, which is well within the range of the known supergiant X-ray pulsars. For observers, the predicted pulse frequency of 1E 1145.1−6141 is

$$\nu(\mathrm{mHz}) = 3.36 + 1.0 \times 10^{-9} T, \tag{2}$$

where T is the desired JD - 2440000.0.

4. Discussion

We have found that the supergiant X-ray pulsar 1E 1145.1−6141 is in a moderately eccentric 14.4 d orbit. On a P_{spin}-P_{orb} diagram, the system resides among the wind-fed supergiant X-ray binaries (Corbet 1986; Waters & van Kerkwijk 1989; Bildsten et al. 1997), as expected from its low X-ray luminosity. The absence of an X-ray eclipse may be used to constrain the binary inclination (and hence the supergiant mass) for a given companion radius R_c. Neglecting the moderate orbital eccentricity, the no-eclipse condition is $R_c/(a_x \sin i) < \cot i$, where we have assumed that the companion mass is much larger than the pulsar

mass. For the range of radii consistent with a B2 Ia supergiant (30–60 $R_\odot$; see de Jager & Nieuwenhuijzen 1987), this gives a maximum inclination angle ranging from 55° to 40°. Assuming a neutron star mass of 1.4 $M_\odot$, this implies a minimum companion mass of 11–22 $M_\odot$.

Pfahl et al. (2002) have noted that massive X-ray binaries can be divided into three broad groups: (i) moderately wide ($P_{\rm orb} \simeq$ 20–100 d) binaries with a significant ($e > 0.3$) eccentricity caused by a neutron star "kick" at birth; (ii) short-period, ($P_{\rm orb} \lesssim 10$ systems in which tidal circularization has resulted in low-eccentricity ($e \lesssim 0.1$) orbits; and (iii) wide ($P_{\rm orb} > 30$ d) binaries with low ($e < 0.2$) eccentricities, which may have experienced a weaker kick at birth. We note that 1E 1145.1−6141 does not fit comfortably into any of these categories, although it appears to be intermediate between groups (i) and (ii). As a 14.4-d binary, it is possible that tidal torques have played some role in reducing the eccentricity caused by the neutron star birth, although this is unlikely to have been a strong effect. It would be interesting to identify more binaries in the 10–20 d range, in order to better understand at what point tidal torques play a substantial role.

Basic research in X-ray astronomy at NRL is funded, in part, by the Office of Naval Research. This work was partially supported by NASA DPR No. S-42631-F.

REFERENCES

Bildsten, L., et al. 1997, ApJS, 113, 367

Chakrabarty, D., Wang, Z., Juett, A. M., Lee, J. C., & Roche, P. 2002, ApJ, 573, 789

Corbet, R. & Mukai, K. 2002, ApJ, in press (astro-ph/0207181)

Corbet, R. H. D. 1986, MNRAS, 220, 1047

de Jager, C. & Nieuwenhuijzen, H. 1987, A&A, 177, 217

Densham, R. H. & Charles, P. A. 1982, MNRAS, 201, 171

Dower, R. G., Apparao, K. M. V., Bradt, H. V., Doxsey, R. E., Jernigan, J. G., & Kulik, J. 1978, Nature, 273, 364

Grebenev, S. A., Pavlinskii, M. N., & Syunyaev, R. A. 1992, Sov. Astron. Lett., 18, 228

Hutchings, J. B., Crampton, D., & Cowley, A. P. 1981, Astron. J., 86, 871

Hutchings, J. B., Crampton, D., Cowley, A. P., & Thompson, I. B. 1987, PASP, 99, 420

Ilovaisky, S. A., Chevalier, C., & Motch, C. 1982, A&A, 114, L7

Jahoda, K., Swank, J. H., Giles, A. B., Stark, M. J., Strohmayer, T., Zhang, W., & Morgan, E. H. 1996, in Proc. SPIE, ed. O. H. Siegmund & M. A. Gummin, Vol. 2808, 59

Lamb, R. C., Markert, T. H., Hartman, R. C., Thompson, D. J., & Bignami, G. F. 1980, ApJ, 239, 651

Mihara, T. 1995, PhD thesis, University of Tokyo

Pfahl, E., Rappaport, S., Podsiadlowski, P., & Spruit, H. 2002, ApJ, 574, 364

Saraswat, P., Mihara, T., Corbet, R., & Ebisawa, K. 1997, ApJ, submitted

van Kerkwijk, M. H., van Paradijs, J., & Zuiderwijk, E. J. 1995, A&A, 303, 497

Waters, L. B. F. M. & van Kerkwijk, M. H. 1989, A&A, 223, 196

White, N. E., Parkes, G. E., & Sanford, P. W. 1978, Nature, 274, 664

White, N. E., Pravdo, S. H., Becker, R. H., Boldt, E. A., Holt, S. S., & Serlemitsos, P. J. 1980, ApJ, 239, 655

AAS LaTeX macros v5.0.

Table 1. RXTE Observations of 1E 1145.1−6141

ObsId	# Obs	Date Range
20130-01-*	6[a]	1997 Jun 21–Jul 30
20130-02-*	4[b]	1997 Sep 24–Aug 16
30108-01-*	40	1998 Jul 4–Aug 12
40079-0[1,2,3]-*	20	1999 Aug 14–Aug 28
40079-04-*	14	2000 Jan 21–Feb 1

[a]1E 1145.1−6141 not detected in 20130-01-05-00

[b]Contaminated by 2S 1145−619 flare, so not used

Table 2. Orbit Parameters

Parameter	Value
$P_{\rm orb}$	14.365 ± 0.002 d
T_0	51008.1 ± 0.4
$a_X \sin i$	99.4 ± 1.8 lt-s
e	0.20 ± 0.03
ω	$-52^\circ \pm 8^\circ$
$f_X(M)$	$5.1 \pm 0.3\ M_\odot$

Note. — Quoted errors are statistical only.

Table 3. 1E 1145.1−6141 Pulse Frequency Measurements

Epoch (MJD)	ν (mHz)	Instrument	Reference
42614	3.3637(2)[a]	*OSO-8*	White et al. 1980
42802	3.3642(7)[a]	*OSO-8*	White et al. 1980
43417	3.3639(1)[a]	*Ariel 5*	White et al. 1980
43484	3.3614(2)[a]	*Ariel 5*	White et al. 1980
44069	3.359(4)[a]	*Einstein*	White et al. 1980
48329.2	3.3681(6)[a]	*Ginga*	Mihara 1995
48330.7	3.3695(6)[a]	*Ginga*	Mihara 1995
48658.8	3.369(1)[a]	*Granat*	Grebenev et al. 1992
49222	3.369(1)[a]	*ASCA*	Saraswat et al. 1997
50625	3.37235(5)	*RXTE*	this work
51018	3.37103(5)	*RXTE*	this work
51410	3.37185(2)	*RXTE*	this work
51570	3.37200(3)	*RXTE*	this work

[a]Not corrected for pulsar orbital motion

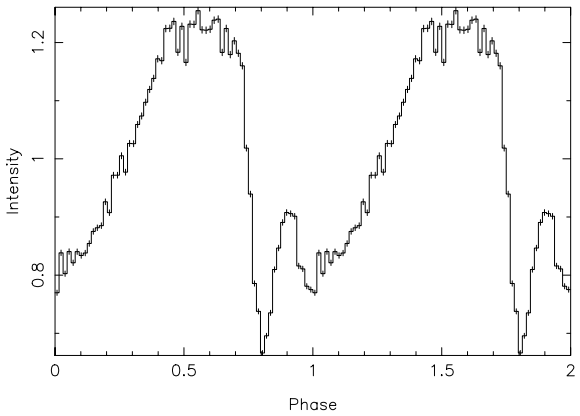

Fig. 1.— Folded light curve (2–10 keV) of 1E 1145.1−6141 with 64 bins from a 14.6 ks observation beginning 1997 June 21 02:28 UTC. Two cycles are shown. Vertical scale is relative count rate.

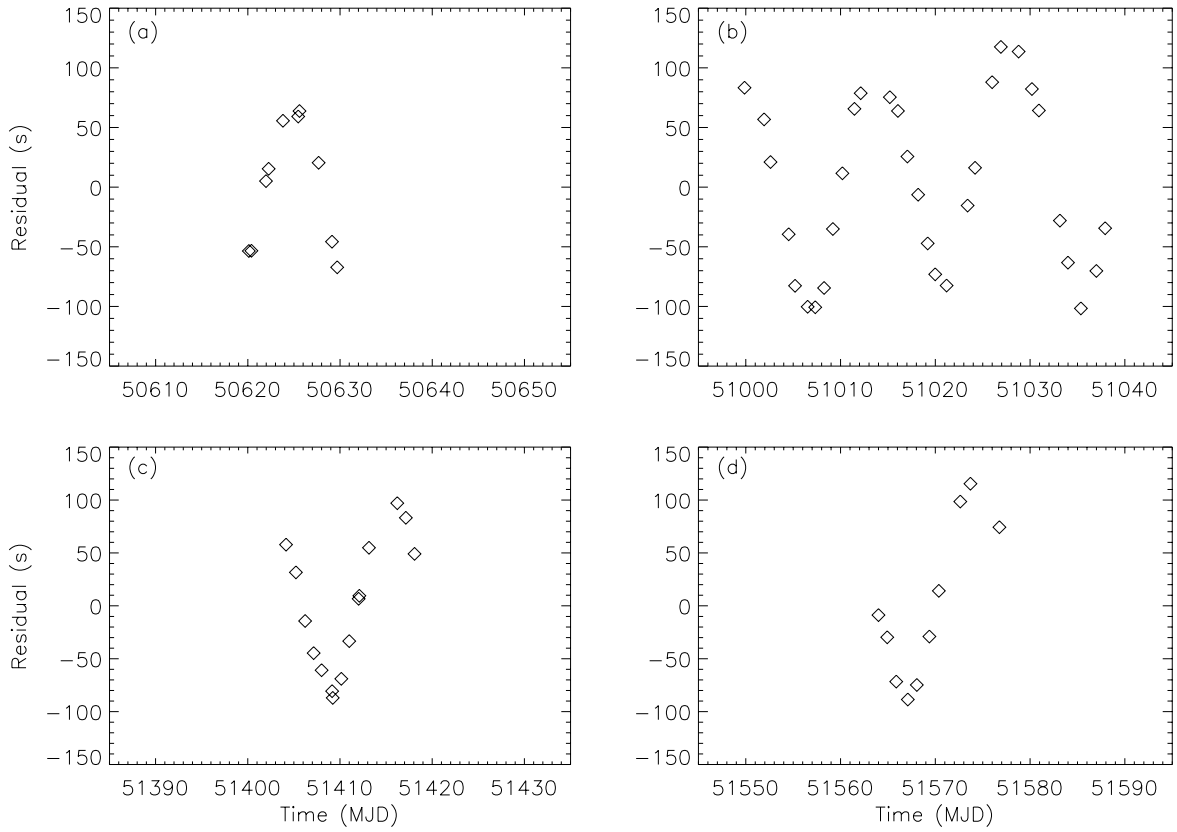

Fig. 2.— Observed pulse arrival times for 1E 1145.1−6141 from four sets of *RXTE* observations after subtracting a constant-period model.

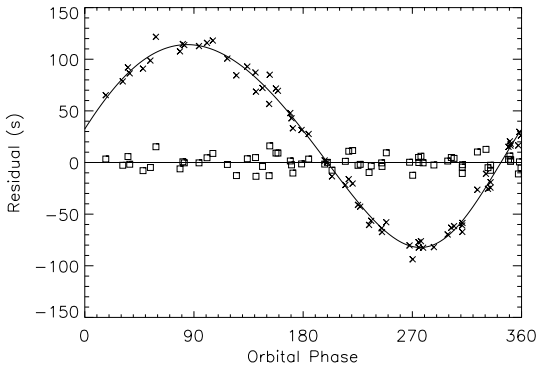

Fig. 3.— Observed pulse arrival time residuals (with each epoch allowed an arbitrary jump in pulse period and phase). The best-fit eccentric orbit solution (from Table 2) is overplotted as a solid line.

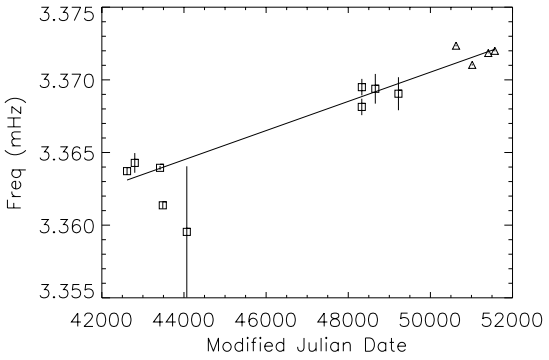

Fig. 4.— Barycentric pulse frequency as a function of time for 1E 1145.1−6141. Squares are previously published data points and triangles are from our *RXTE* observations.